



Available online at www.sciencedirect.com

ScienceDirect

Soils and Foundations 65 (2025) 101661



www.elsevier.com/locate/sandf

Technical Paper

Experimental analysis of reinforcement methods for stone column foundations

Lihua Li a,c, Jinlin Li a,c, Zhiqi Zhan b,*, Yilin Gui d, Juqiang Liu a,c

- ^a School of Civil Engineering, Architecture and Environment, Hubei University of Technology, Key Laboratory of Health Intelligent Perception and Ecological Restoration of River and Lake, Ministry of Education, Wuhan 430068, China
- ^b Department of Civil and Environmental Engineering, The Hong Kong Polytechnic University, Hung Hom, Kowloon, Hong Kong
 ^c Hubei Key Laboratory of Environmental Geotechnology and Ecological Remediation for Lake & River, Hubei University of Technology, Wuhan,
 Hubei 430068, China

Received 11 March 2025; received in revised form 26 June 2025; accepted 8 July 2025 Available online 18 July 2025

Abstract

Geosynthetic-reinforced stone columns can significantly improve weak foundations. While previous studies have focused on the individual effects of vertical or horizontal reinforcement, the combined influence of both on stone column foundation performance remains poorly understood. Through physical model tests, this study investigated the effects of various reinforcement methods on the bearing capacity and deformation characteristics of stone column foundations, with a particular focus on the combined reinforcement in enhancing their performance, addressing this research gap. This study encompasses different enhancement lengths, horizontal reinforcement spacings, and combinations of reinforcement methods. Experimental results demonstrate that geosynthetics significantly limit radial deformation and improve the bearing capacity of stone column foundations. Notably, the bearing capacity increases with reduced reinforcement spacing and extended enhancement length. Among all the reinforcement types tested in this study, the full-length (L) vertical reinforcement demonstrated the most significant impact. Additionally, the study examines stress transfer and lateral stress distribution within the stone columns, revealing that as the load increases, the stress ratio at the stone column base and lateral stress rises, with lateral stress peaking at a depth of 2.5D from the surface. This behaviour aligns with the deformation patterns observed in the model tests.

© 2025 Japanese Geotechnical Society. Published by Elsevier B.V. This is an open access article under the CC BY-NC-ND license (http://creativecommons.org/licenses/by-nc-nd/4.0/).

Keywords: Geosynthetics; Ground improvement; Gravel; Foundations; Model tests

1. Introduction

Stone columns can improve the performance of weak foundations by enhancing the bearing capacity (Schweiger and Pande, 1986; Lajevardi et al., 2018; Benmebarek et al., 2018; Hataf et al., 2020; Deshpande et al., 2021), and their effectiveness primarily depends on the lateral confining pressure exerted by the surrounding

E-mail addresses: lilihua466@163.com (L. Li), zhiqi.zhan@connect.polyu.hk (Z. Zhan), yilin.gui@qut.edu.au (Y. Gui).

^d School of Civil and Environmental Engineering, Queensland University of Technology, Gardens Point, Brisbane, QLD 4000, Australia

soils. However, in many cases, the enhancement by stone columns is limited due to low lateral confining pressure (Sharma et al., 2004). The deformation of stone columns under external loading can also reduce their capacity enhancement (Indraratna et al., 2015). For instance, embankments constructed on stone column foundations can experience sliding failure due to the lateral movement of stone columns and soil under wide flexible loading (Sharma et al., 2004; Orekanti and Dommaraju, 2019). To address these limitations, geosynthetics have been used to reinforce stone columns, overcoming the loss of capacity

^{*} Corresponding author.

enhancement and reducing settlement (Elsawy, 2013; Wu and Hong, 2014; Bazzazian Bonab et al., 2020).

Van Impe (1989) first introduced the method of encasing stone columns with geosynthetic materials to enhance lateral confinement. Subsequently, many studies have investigated geosynthetic-reinforced stone columns, proposing three reinforcement methods. The first method involves vertical reinforcement by wrapping the stone column with geosynthetics (Verma et al., 2018; Rathod et al., 2021). The second method employs horizontal reinforcement by incorporating geogrids in layers between the stone column fill (Sharma et al., 2004; Hasan and Samadhiya, 2018). The third method involves adding a specific thickness of sandy soil layer on top of the stone column foundation after the installation of stone columns in the weak soil layer, followed by reinforcement within the upper sandy soil layer (Deb et al., 2011; Dash and Bora, 2013). Among these, the first two methods (vertical and horizontal reinforcements) are the most widely used.

Vertical reinforcement effectively prevents cracking and collapse (bulging deformation) of stone column foundations under high vertical loads. Additionally, it helps maintain superior drainage performance by preventing the loss of aggregates (Yoo and Lee, 2012; Thakur et al., 2021). Studies indicate that both encasement length and geotextile stiffness significantly influence pile performance. Optimal encasement lengths of 2 to 3 times the pile diameter minimize settlement and maximize stiffness (Yoo and Lee, 2012; Tandel et al., 2014; Hataf et al., 2020).

The higher stiffness of the geotextile reduces lateral stress transfer to the surrounding soil, making the pile performance less dependent on the surrounding ground condition (Murugesan and Rajagopal, 2006; Gniel and Bouazza, 2010; Tandel et al., 2014). However, (Malarvizhi, 2007) found that when stiffness exceeds 2000 kN/m, its improvement effect diminishes. Additionally, pile diameter affects the effectiveness of wrapping materials: larger diameters increase bearing capacity, while smaller diameters enhance constraint effects (Murugesan and Rajagopal, 2010; Ghazavi and Afshar, 2013; Nazari Afshar and Ghazavi, 2014). Zhang and Zhao (2015) emphasized that geotextile stiffness selection should consider column diameter and spacing due to their impact on deformation behavior.

Horizontal reinforcement enhances the horizontal bearing capacity and integrity of stone column foundations by increasing the peak shear strength at geosynthetic-aggregate interfaces, controlling radial deformation, and improving resistance to seismic and wind loads (Ali et al., 2012; Dinarvand and Ardakani, 2018; Pereiro-Barceló et al., 2022). The performance of stone column foundations can be significantly improved by horizontally laying geogrids at fixed intervals within the gravel pile fill (Zhang and Zhao, 2015; Naeini and Gholampoor, 2019). Optimal reinforcement performance is achieved when the spacing of the geosynthetic layers equals half of the pile diameter (Ali et al., 2012).

The key literatures are summarized in Table 1. In summary, previous studies have investigated the individual effects of horizontal and vertical reinforcements, and each has its unique advantages. Practically, combined reinforcement integrates the benefits of both horizontal and vertical methods, enhancing the integrity and bearing capacity of stone columns through a spatial structural approach. However, to the best of the authors' knowledge, studies on the effects of combined vertical and horizontal reinforcement on the performance of stone column foundations remain limited. To address this research gap, this study conducted static load model tests on stone column foundations, investigating various reinforcement methods. Special attention was given to how combined reinforcement influences the performance of stone column foundations. This study analyzed the effects of different reinforcement combinations, encasement lengths, and reinforcement spacings on bearing capacity, stress concentration ratio, and deformation of the stone columns. The findings of this research provide a basis for the widespread application of reinforced stone columns in engineering practice.

2. Test materials and methods of physical model test

2.1. Test materials

The materials used in the tests primarily consist of sandy soil, granite gravel, geotextiles, and geogrids. The sandy soil served as the model foundation fill, with a maximum particle size of 5 mm. The granite gravel was crushed and sieved through 2 mm, 5 mm, and 10 mm screens, resulting in two particle size groups: 2–10 mm and 5–10 mm. The 2–10 mm range was used as filler for the stone columns, while the 5–10 mm range was utilized to fill the lower layer of the model (hard layer).

The parameters of sandy soil and granite gravel are presented in Table 2. According to GB/T50123-2019, sandy soil and gravel are classified as GP and SP, respectively. The particle size distribution is presented in Fig. 1. The coefficient of uniformity (Cu) and coefficient of curvature (Cc) for sandy soil and gravel fill can be calculated by Eqs. (1) and (2):

$$C_u = \frac{d_{60}}{d_{30}} \tag{1}$$

$$C_c = \frac{d_{30}^2}{d_{60} \times d_{10}} \tag{2}$$

where d_{60} is the constrained particle size, at which 60 % of the soil mass is finer on the particle size distribution curve; d_{30} is the particle size at which 30 % of the soil mass is finer on the particle size distribution curve; and d_{10} is the effective particle size, at which 10 % of the soil mass is finer on the particle size distribution curve. All of these parameters can be obtained from Fig. 1.

The maximum dry density and optimum moisture content of the materials was determined through a standard

Table 1
Key studies on geosynthetic-reinforced stone column foundations.

Reinforcement Type Study		Key Findings		
Vertical	Van Impe. (1989)	Introduced geosynthetic encasement for lateral confinement.		
	Murugesan et al. (2006)	Higher geotextile stiffness improves pile performance.		
	Yoo and Lee. (2012)	Vertical encasement prevents aggregate loss and enhances drainage.		
	Tandel et al. (2014)	Geotextile stiffness reduces lateral stress transfer.		
	Verma et al. (2018)	Wrapping prevents cracking and collapse under high loads.		
	Hataf et al. (2020)	Enhanced bearing capacity with optimal encasement length (2–3 times pile diameter).		
Horizontal	Sharma et al. (2004)	Geogrids increase shear strength and control radial deformation.		
	Deb et al. (2011)	Sandy layer reinforcement reduces settlement.		
	Ali et al. (2012)	Optimal geogrid spacing enhances shear strength and horizontal bearing capacity.		
Vertical/Horizontal	Elsawy et al. (2013)	Geosynthetics reduce settlement and enhance capacity for both vertical and horizontal reinforcement.		
	Zhang and Zhao. (2015)	Geotextile stiffness selection should consider column diameter and spacing for optimal performance.		
	Dinarvand and Ardakani. (2018)	Improved resistance to seismic and wind loads.		
	Bazzazian et al. (2020)	Geosynthetic reinforcement overcomes capacity loss.		

Table 2 Characteristics and properties of sandy soil and granite gravel.

	Sandy soil	Granite gravel (2-10 mm)(Column fill)	Granite gravel (5–10 mm)(Hard layer)
Category	SP	GP	GP
Coefficient of uniformity, C_u	4.62	0.83	0.88
Coefficient of curvature, C_c	0.81	2.01	2.15
Elastic modulus, E (MPa)	17	38	41
Poisson's ratio, v	0.25	0.2	0.35
Cohesion, c (kPa)	2	8	8
Friction angle, φ (°)	35	42	40
Optimal water content (%)	12.4	5.0	5.6
Maximum dry density (g/cm ³)	1.88	1.76	1.79

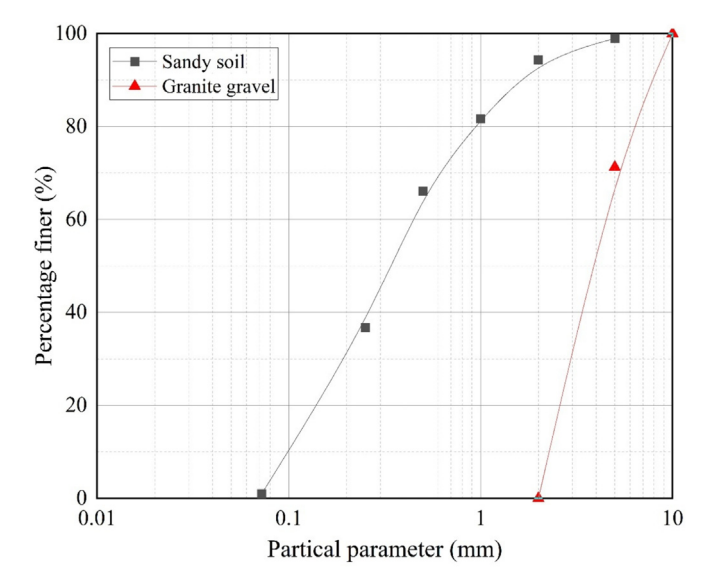


Fig. 1. Particle size distribution of the test materials.

compaction test, following the GB/T50123-2019 (Cai et al., 2019). Sandy soil was sampled using the quartering method (approximately 50 kg), air-dried, passed through a 20 mm sieve, mixed uniformly, and tested for initial moisture content. Gravel was sieved and directly tested for initial mois-

ture content. After estimating the optimum moisture content, five samples were prepared at 2 % moisture content intervals, mixed uniformly, and sealed for 24 h to ensure even moisture distribution. A portion of the sample was placed into the compaction cylinder in three layers of equal height, with each layer compacted 94 times. After compaction, the top was leveled, the total mass was measured to calculate the wet density, and three representative samples were taken to determine the moisture content. The test was repeated for the remaining samples.

The compaction test results for the model test are presented in Fig. 2. The maximum dry density and optimum moisture content of the material are determined from the peak point of the curve, where the corresponding abscissa indicates the optimum moisture content, and the corresponding ordinate represents the maximum dry density. Cohesion and friction angle were determined through triaxial testing as reported by (Lade and Duncan, 1975), while elastic modulus and Poisson's ratio was adopted as a typical value from (Kulhawy and Mayne, 1990).

The stone columns were reinforced vertically with geotextile (glass fibre) and horizontally with biaxial geogrids, with the geotextile mesh size being 2×2 mm (Li et al., 2023). conducted tensile tests on the geosynthetics following ISO 13019. The physical properties of the geotextile and geogrid are detailed in Tables 3 and 4, respectively.

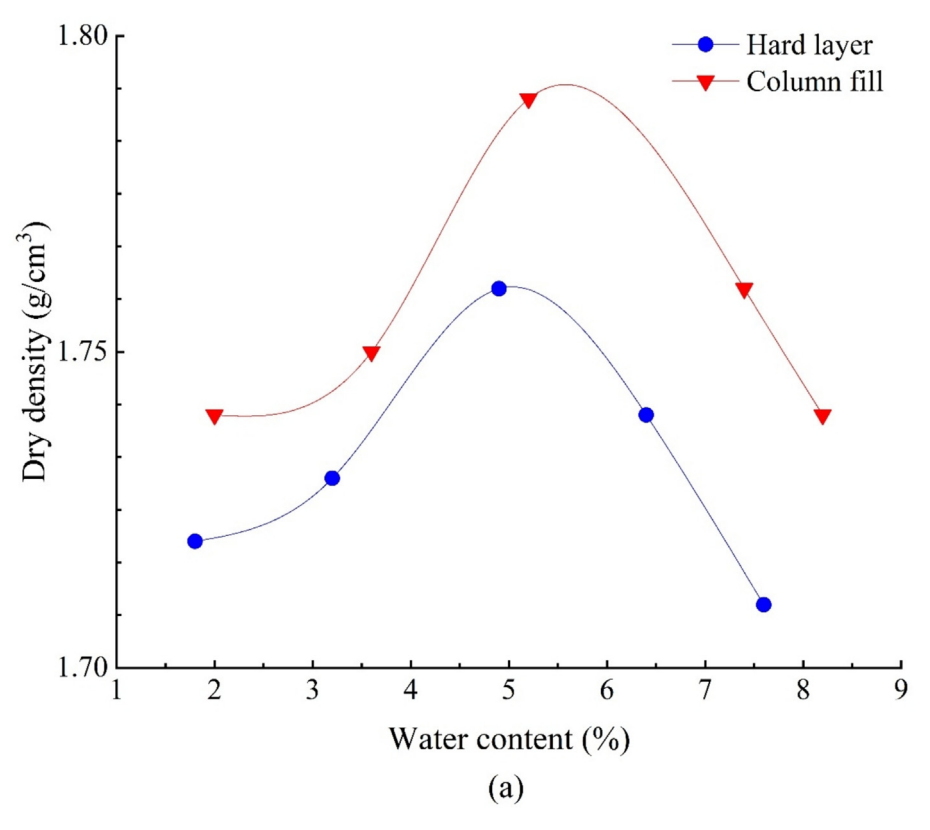


Fig. 2. The compaction curve of (a) Granite gravel; and (b) Sandy soil.

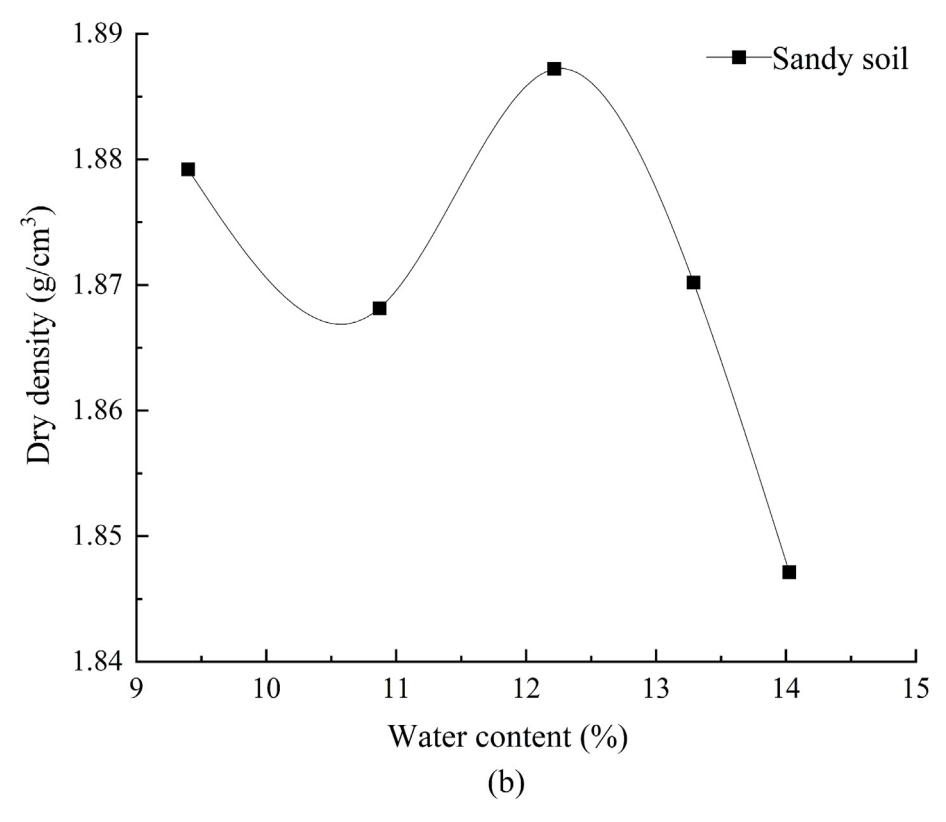


Fig 2. (continued)

Table 3 Characteristics and properties of geotextile.

Material	Glass fibre
Ultimate tensile strength (kN/m)	23.8
Strain at ultimate tensile strength (%)	25.2
Tensile strength at 2 % elongation (kN/m)	2.3
Tensile strength at 5 % elongation (kN/m)	6.8
Stiffness (KN/m)	136

Table 4 Characteristics and properties of biaxial geogrid.

	Unit weight (g/m²)	400 ± 4
Horizontal	Tensile strength (kN/m)	30
	Ultimate elongation (%)	≤ 13
	Tensile strength at 2 % elongation (kN/m)	≥ 15
	Tensile strength at 5 % elongation (kN/m)	≥ 15
Vertical	Tensile strength (kN/m)	30
	Ultimate elongation (%)	≤ 16
	Tensile strength at 2 % elongation (kN/m)	≥ 11
	Tensile strength at 5 % elongation (kN/m)	≥ 13

2.2. Experimental setup

The experimental setup comprises a manually loaded counterforce frame apparatus, consisting of a counterforce frame, hydraulic jack, and a digital display system (DH5922D Dynamic Signal Test and Analysis System), as illustrated in Fig. 3. The device features a maximum stroke of 200 mm, a thrust capacity of 20 t, and an applied pressure of 63 MPa. The circular loading plate utilized in this investigation has a diameter of 200 mm, while the internal dimensions of the model box are 800 mm (length) \times 800 mm (width) \times 900 mm (height). The dimensions of the model box were determined based on the loading plate size, ensuring that the width of the model box is no less than four times the maximum diameter of the loading plate to satisfy the boundary conditions for static load testing (Li et al., 2023).

The schematic diagram of the physical model test is given in Fig. 4. The sensors employed in this study include a linear displacement meter, earth pressure cells, and pull wire displacement sensors. The linear displacement meter has a maximum measurement range of 200 mm, allowing for real-time monitoring of settlement within the loading zone. The earth pressure cells measure 28 mm × 10 mm, with a measurement range of 300 kPa, enabling precise assessment of soil pressure. The pull wire displacement sensors are employed to quantify the lateral deformation of the stone column, with one end anchored to the column's lateral surface and the other secured to the inner wall of the model box.

2.3. Test programme

This study investigated three reinforcement methods for stone columns, as shown in Fig. 5. Vertical reinforcement (Fig. 5(a)) uses geosynthetic inclusions to enhance lateral

restraint, reducing settlement and aggregate loss (Yoo and Lee, 2012; Hataf et al., 2020). Horizontal reinforcement (Fig. 5(b)) employs stratified geogrids (D/3 to D spacing) to improve stress distribution and shear resistance (Ali et al., 2012; Zhang and Zhao, 2015). Combined reinforcement (Fig. 5(c)) integrates both, boosting bearing capacity and deformation control through synergistic confinement and interlocking.

The effects of encasement length, reinforcement spacing, and reinforcement combinations on the bearing capacity and deformation of stone column foundations were investigated through physical model testing. The vertical geosynthetic reinforcement of the stone columns was implemented using glass fiber geotextile, with two configurations: full-height encasement (L = 600 mm) and halfheight encasement (L/2 = 300 mm). The half-height encasement extended from the base up to 300 mm, while the full-height encasement provided comprehensive radial confinement from the base to the top of the column. Horizontal reinforcement was achieved by placing biaxial geogrids at intervals of D (100 mm), 2D/3 (66.67 mm), and D/3 (33.33 mm). The composite reinforcement configuration combined 300 mm vertical encasement with horizontal geogrid spacing of either 100 mm (L/2 + D) or 66.67 mm (L/2 + 2D/3) in the upper section, therebyenhancing load transfer capacity through synergistic effects. For comparative analysis, a pure sandy soil foundation without stone columns and a stone column foundation with unreinforced stone columns were also tested. The detailed test programme is presented in Table 5 (Li et al., 2023).

The diameter of the stone column prototype typically ranges from 600 to 1000 mm (Debnath and Dey, 2017). In practical applications, the length-to-diameter ratio (L/D) of stone columns varies from 5 to 20 (Shahu and Reddy, 2011; Hasan and Samadhiya, 2017). In this study, a stone column with a diameter of 100 mm was selected, maintaining a similarity ratio of 10 (corresponding to 1000 mm in prototype size), with the column length set at 600 mm (L/D = 6).

2.4. Test procedures

The details of the physical model are shown in Fig. 4. The model construction process is as follows:

(1) The hard layer was constructed by filling granite crushed stones (particle size 5–10 mm) in two layers under dry conditions, with each layer controlled to a thickness of 50 mm. After each fill, the layer was compacted using a standardized compaction effort to achieve 95 % of the maximum dry density, ensuring uniform density and stability. The physical and mechanical parameters of the resulting hard layer, including dry density, shear strength, and gradation, were measured and are presented in Table 2 (right-hand column).

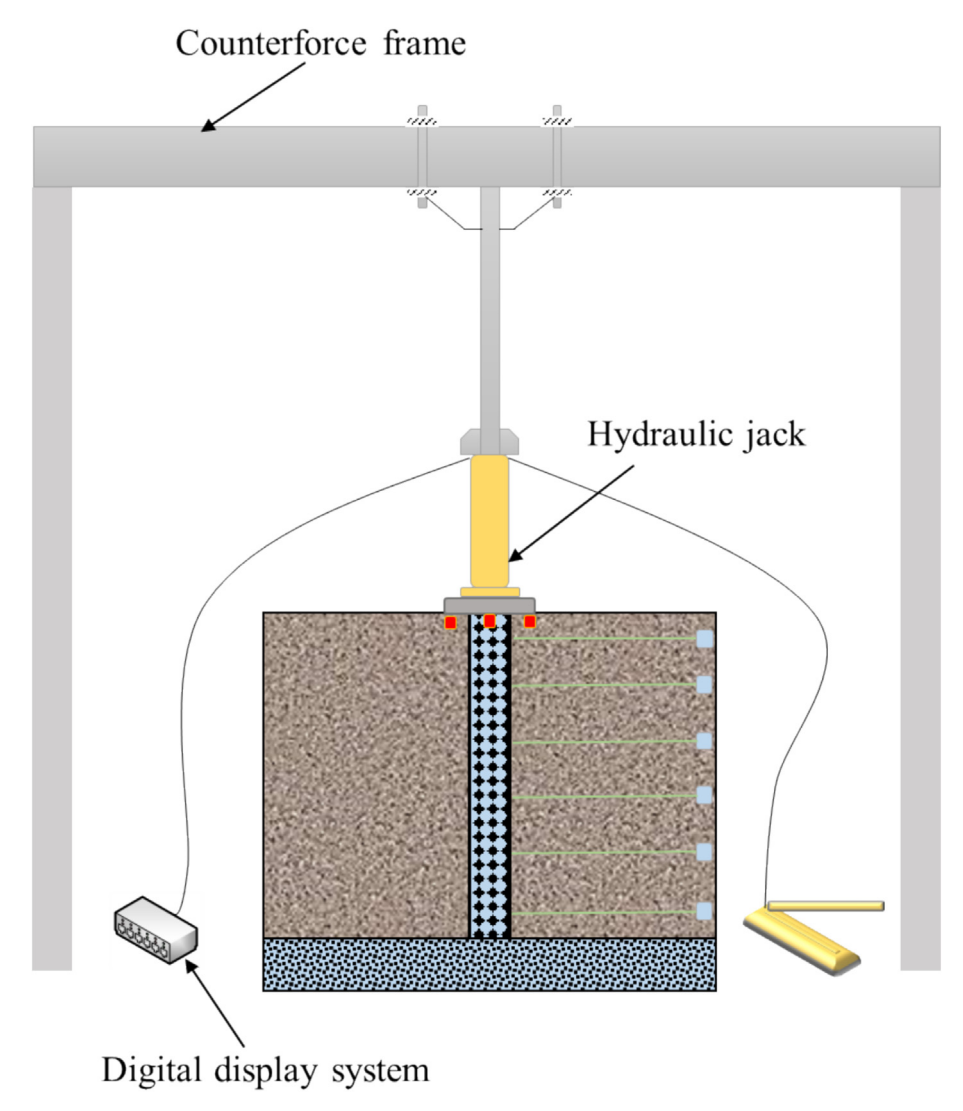


Fig. 3. Manually loaded counterforce frame apparatus.

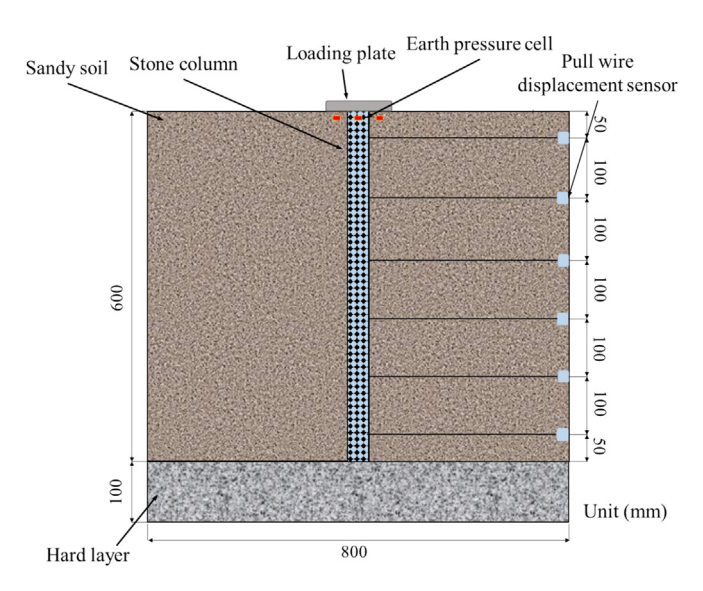


Fig. 4. Schematic diagram of the physical model test (after Li et al., 2023).

- (2) After completing the hard layer, a 700 mm long, 100 mm diameter thin-walled polyvinyl chloride (PVC) pipe was centrally fixed on the upper surface of the hard soil. Lubricating grease was uniformly applied to both the inner and outer walls of the pipe to reduce friction between the PVC pipe and the sandy soil. Additionally, two steel wires were fixed to the top of the pipe to facilitate the removal of the PVC pipe after the stone column construction was completed.
- (3) Sandy soil was placed in layers on top of the hard layer, with each layer approximately 100 mm thick. The sandy soil in the model ground was subjected to heavy compaction to achieve a relative density of 75 %, corresponding to approximately 91 % of the maximum dry density, which is a typical value in practical engineering applications. This classifies the soil as dense soil (Choo, 2018; Zhan et al., 2025). The soil's water content is 2.8 %, consistent with its natural moisture content. The moisture content was

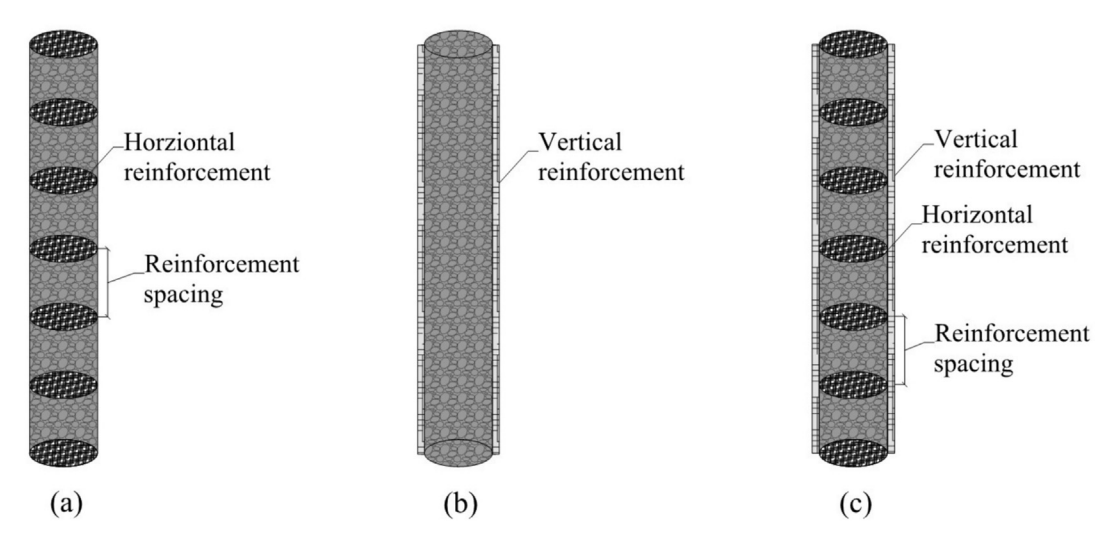


Fig. 5. Diagrams of (a) Horizontal reinforcement, (b) Vertical reinforcement, and (c) Combined reinforcement.

Table 5 Summary of the test programme.

Group number	Reinforcement type	Column length (mm)	Column diameter (mm)	Encasement length	Reinforcement spacing (mm)
1	Pure sandy soil	_	_	_	_
2	Unreinforced	600	100	_	_
3	Vertical reinforcement	600	100	L/2	_
4		600	100	L	_
5	Horizontal reinforcement	600	100	_	D
6		600	100	_	2D/3
7		600	100	_	D/3
8	Combined reinforcement	600	100	L/2	D
9		600	100		2D/3
10		600	100		D/3
11		600	100	L	D
12		600	100		2D/3
13		600	100		D/3

not adjusted to the optimum value to better simulate the natural field conditions, ensuring a more realistic representation of practical engineering scenarios. Additional details of the parameters are provided in Table 2 (left-hand column). After filling each layer, the surface was levelled, and pull wire displacement sensors were installed. To minimize measurement errors caused by friction between the pull wire and the sandy soil layer, the end of the pull wire that contacts the column was wrapped with 2 cm of insulating tape. The wire is then passed through a PVC pipe with an inner diameter of 20 mm and a length of 300 mm to ensure it remains taut. This process was repeated until the design height was achieved.

(4) After installing the pipe and compacting the surrounding soil, the column-filling material was poured into the PVC pipe in six layers, each 100 mm thick. During the construction of each layer, a rubber mallet was gently used to tap the pipe wall for compaction. After every two layers of filling material, the PVC pipe was withdrawn 50 mm. Once the filling was complete, the PVC pipe was fully extracted.

The horizontal reinforcement material, specifically the biaxial geogrid, was cut to dimensions slightly smaller than the diameter of the stone column. It was laid horizontally according to the required reinforcement spacing. The vertical reinforcement material, consisting of glass fibre geotextile, was wrapped around the exterior of a PVC pipe and arranged together with the PVC pipe during the model preparation. When the PVC pipe was removed, the geotextile remained wrapped around the exterior of the stone column.

The installation process of horizontal reinforcement in actual construction includes foundation preparation (clearing debris, stabilizing weak soil), laying geogrids with precise alignment using GPS positioning or laser-based tools (typically achieving a planar error ≤ 5 cm), overlapping connections with 30–50 cm lap joints secured by U-shaped nails or hot welding, pre-tensioning with hydraulic jacks, edge fixation, and protective backfilling in layers (≤ 30 cm). High precision is supported by automated laying systems (commonly achieving 2–5 cm accuracy) or skilled manual techniques, supplemented by stress monitoring using sensors or traditional gauges, depending on project

scale and budget (Lees and Matthias, 2019). Challenges include environmental factors (e.g., wind, rain), material relaxation, and manual operation variability. To address these, factory-prefabricated geogrid modules, real-time sensor adjustments, and post-installation checks like radar scanning and peel tests can be employed, ensuring compliance with technical standards.

The radial effect of the stone column typically extends 2 to 4 times the column radius (Chummar, 1975; Castro, 2014). Considering the radius of the test stone column is 50 mm, a circular loading steel plate with a radius of 100 mm and a thickness of 15 mm was used as the foundation to apply the load.

After constructing the model, a staged loading method was employed. The next load level was applied once the foundation's settlement stabilized under a specific load, defined as less than 0.1 mm of settlement within one hour. If the foundation's settlement did not reach a stable condition or continued to increase significantly after 2 h of loading, this indicated failure, and loading ceased. At this point, the corresponding value was defined as the ultimate load.

3. Test results and discussion

3.1. Bearing capacity of foundation

This study selected two encasement lengths, L/2 and L, to investigate the effect of vertical encasement length on the bearing capacity of the foundation. The corresponding load-settlement (P-S) curves are presented in Fig. 6. The results indicate that the pure sandy soil foundation and the unreinforced stone column foundation failed at loads of 178 kPa and 256 kPa, respectively. Compared to the unreinforced stone column foundation, the bearing capacities of the stone columns reinforced with geotextiles of lengths L/2 and L increased by 38 % and 51 %, respectively. This demonstrates that the vertical reinforcement method significantly enhances the foundation's bearing capacity. The bearing capacity increases with the length of the vertical encasement.

Fig. 6 also reveals distinct deformation patterns between the pure sandy soil foundation and the stone column foundation. In the pure sandy soil foundation, the relationship between load and settlement is typically linear. However, in the stone column foundation, the initial slope of the P-S curve is relatively small, with accelerated settlement occurring only after the load exceeds a certain threshold (125 kPa for the unreinforced stone column foundation). This effect is more pronounced in the stone column foundation with vertical reinforcement. Before reaching the threshold (approximately 160 kPa for both reinforcement scenarios), the increase in settlement is very gradual. Subsequently, the slopes of the P-S curves for all stone column foundations become approximately the same. Notably, as the encasement length increases, the foundation can sustain greater loads at the same settlement, thereby validating the effectiveness of vertical reinforcement.

The slope changes in the P-S curve, observed in Fig. 6 around 150–200 kPa for the vertical reinforced cases (L and L/2), indicates yielding of the stone column foundation. This is characterized by localized plasticization of the pile-soil composite and the failure of lateral confinement provided by the geotextile, leading to a transition into a plastic deformation phase while retaining residual bearing capacity. Similar yielding behavior in geosynthetic-reinforced stone columns has been documented by Murugesan and Rajagopal (2006). This yielding threshold can guide the optimization of reinforcement parameters, such as geotextile stiffness and confinement density, to enhance stone column foundation performance.

Three reinforcement spacings (D, 2D/3, and D/3) were selected to evaluate the influence of horizontal reinforcement spacing on bearing capacity. The corresponding load-settlement curves are presented in Fig. 7. The bearing capacity of the foundations increased by 13 %, 26 %, and 39 % for horizontal reinforcement spacings of D, 2D/3, and D/3, respectively, compared to the unreinforced stone column foundation. This indicates that horizontal reinforcement significantly enhances bearing capacity and reduces settlement, with improvements becoming more pronounced as reinforcement spacing decreases. This behaviour can be attributed to the interlocking effect between the geogrid and the column filler, which intensifies with reduced spacing, resulting in increased friction between the filler and the geogrid. It is also noteworthy that there is no significant difference in the settlement values of stone columns reinforced with D and 2/3D spacing geogrids until the load reaches 150 kPa.

In Figs. 6 and 7, the yield load for both vertical (L, L/2) and horizontal (D/3, 2D/3, D) geosynthetic reinforcements appears at around 150–200 kPa, indicating similar confinement effects. Both types of reinforcement improve the lateral restraint of the stone column by using their tensile strength (Table 4) to resist deformation until the yield point, where plastic deformation starts. This similarity is because the tensile strength of the geosynthetics and their interaction with the soil mainly control the behaviour at low strain levels. Wu and Hong (2008) also found that the confinement effect in reinforced stone columns is mainly determined by the tensile properties of the geosynthetics, rather than their orientation. However, after yielding, the failure mechanisms are different due to the different ways the load is distributed according to the reinforcement direction.

To investigate the effect of combined vertical and horizontal reinforcement on bearing capacity and to determine the optimal combination, the load-settlement characteristics for six different combinations, as listed in Table 5, are presented in Fig. 8. All geosynthetic-reinforced stone column foundations exhibited improved bearing capacity and reduced settlement compared to unreinforced stone column foundations. When the load was below 100 kPa, the differences in the load-settlement curves for the various combinations were relatively minor, and the influence of

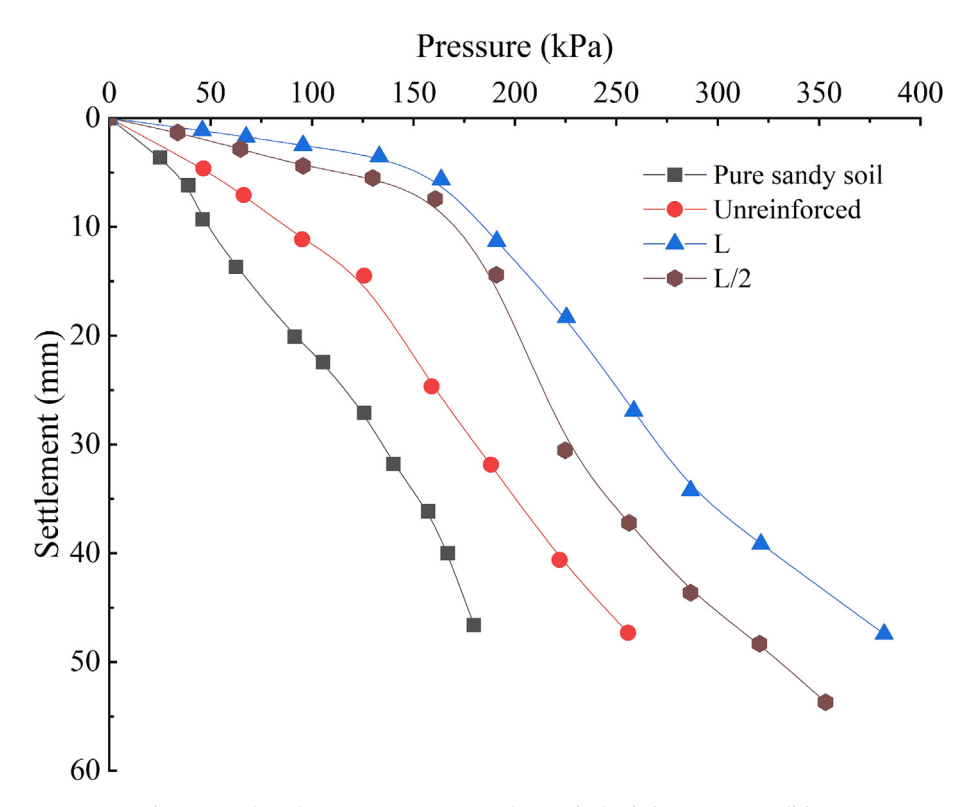


Fig. 6. Load-settlement (P-S) curves under vertical reinforcement conditions.

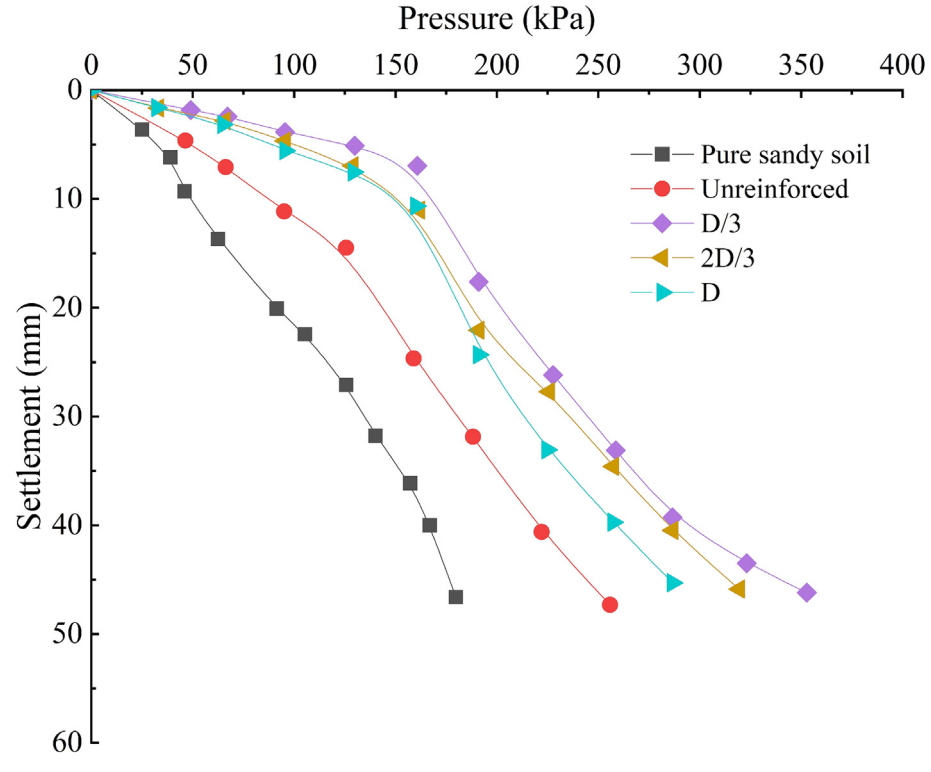


Fig. 7. Load-settlement (P-S) curves under horizontal reinforcement conditions.

different reinforcements was not pronounced. However, as the load increased, the variations in the curves became more evident. The (L/2 + 2D/3) combination demon-

strated the most effective reinforcement, consistently resulting in lower settlement compared to the other combinations. Although the bearing capacity for the (L + D), (L/2 + D/3), and (L/2 + 2D/3) combinations were similar, the (L/2 + 2D/3) combination achieved a more significant reduction in settlement than the other two. Therefore, the (L/2 + 2D/3) reinforcement combination was the most optimal in this study. Conversely, the (L + 2D/3) combination exhibited the poorest performance, with the lowest bearing capacity (320 kPa) and the highest settlement (53 mm) among the tested combinations. The bearing capacity for the (L/2 + D) and (L + D/3) combinations were similar, showing increases of 38 % and 39 %, respectively, compared to the unreinforced stone column foundations.

The experimental results shown in Figs. 6–8 indicated that for vertical reinforcement, the optimal encasement length was L. For horizontal reinforcement, the spacing of D/3 proved to be the most effective design. In the case combined reinforcement, the configuration (L/2 + 2D/3) was identified as optimal. To compare the impact of different reinforcement methods on the bearing capacity of stone column foundations, the load-settlement curves for the three optimal reinforcement strategies are presented in Fig. 9. The L-length vertical reinforcement demonstrated superior performance compared to the D/3 horizontal reinforcement and the (L/2 + 2D/3) combined reinforcement. Notably, the bearing capacity for the combined reinforcement (L/2 + 2D/3) was very close to that of the vertical reinforcement (L), being approximately 35 % greater than that of the horizontal reinforcement (D/3).

This enhancement is attributed to the ability of vertically reinforced stone columns to mobilize circumferential stress from the glass fiber geotextiles, thereby improving lateral stress resistance and overall bearing capacity. Consequently, the load applied at the top is more effectively transferred to the base of the stone column. As the load increases, the stress in the lower section of the vertically reinforced stone column correspondingly rises, highlighting the advantages of full-length encasement.

Although the combined reinforcement (L/2 + 2D/3) integrates the benefits of both horizontal and vertical reinforcement, the relatively short vertical encasement length (L/2) limits its effectiveness. Reducing the distance between reinforcing layers enhances frictional and interlocking interactions between the stone column materials and the reinforcement (Ghazavi et al., 2018). This configuration prevents lateral movement of the stone column aggregates. However, when the reinforcement spacing increases to 2D/3, lateral movement of the stone column material occurs, diminishing the improvement in bearing capacity and settlement.

3.2. Stone column deformation

To investigate the deformation of the stone column along its depth, Fig. 10 depicts the radial deformation rate, defined as the ratio of the increase in column diameter to its original diameter. The diameter increase, an experimental parameter, was measured using pull-wire displacement sensors, as shown in Fig. 4.

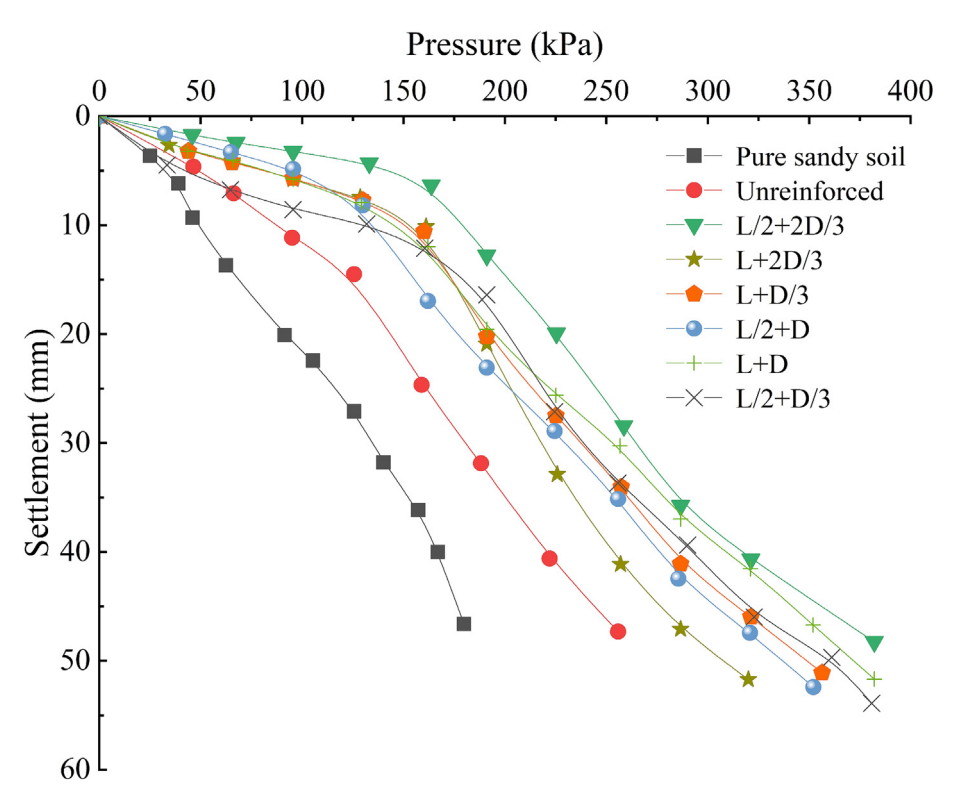


Fig. 8. Load-settlement (P-S) curves under combined reinforcement conditions.

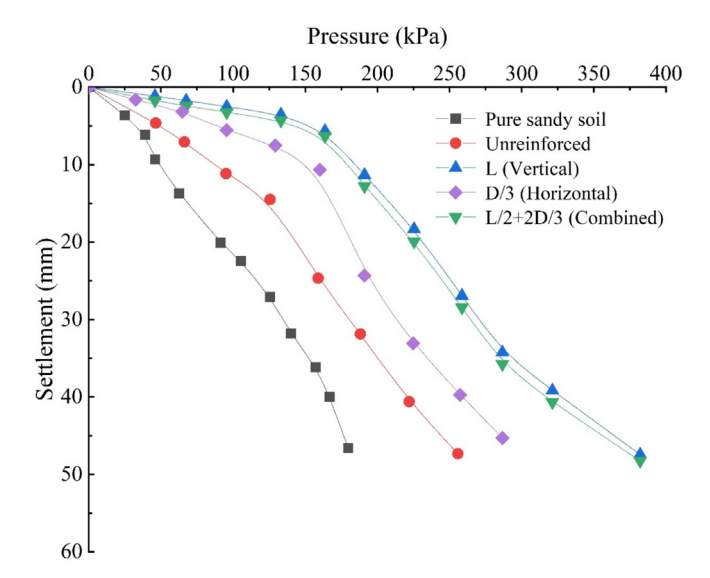


Fig. 9. Load-settlement (P-S) curves under optimal vertical, horizontal, and combined reinforcement types.

The deformation observed in Fig. 10 primarily occurred within 350 mm (3.5D) from the top of the column. The maximum radial deformation for the column with a vertical encasement length of L/2 was recorded at 3.5D from the top, while all other configurations exhibited maximum deformation at 2.5D. Notably, the maximum radial deformation rate of the unreinforced column reached 8.5 %. In contrast, the maximum deformation rate for the geosynthetic-reinforced column was only 3.9 % (specifically for the L/2 + 2D/3 reinforcement), indicating that the geosynthetics significantly constrained the radial deformation of the column. Among all reinforcement methods, the vertical encasement length L exhibited the smallest maximum radial deformation rate at 2.1 %. The minimum deformation rate for horizontal reinforcement was 3.1 %. still exceeding that of the vertical reinforcement at 2.3 %. This difference arises because the vertical reinforcement provided by geotextiles offers additional lateral support, effectively limiting lateral deformation more than horizontal reinforcement.

As shown in Fig. 10, the reinforcing material reduces the radial deformation rate of the stone column. Its mechanism involves multi-physical interactions: Geosynthetic materials establish lateral constraints via the "hoop effect," reducing radial strain by approximately 50 % through passive resistance to particle displacement. The interfacial friction between the reinforcing material and the aggregate, along with mechanical interlocking, forms a composite system that redirects particle motion into an ordered mode. Additionally, the redistribution of tensile stress converts local shear stress into circumferential tension, decreasing core shear stress by 30–40 % through stress bridging, while the inherent stiffness of the reinforcing materials generates a counterforce, resisting deformation via stored strain energy. These coupled mechanisms enhance load transfer

efficiency and deformation resistance through synergistic constraint-friction-stiffness interactions (Wu and Hong, 2008).

Furthermore, the deformation rate of the unreinforced stone column showed considerable variation along its length. As illustrated in Fig. 10, the radial deformation rate of the unreinforced stone column was predominantly concentrated in the upper half. In contrast, the geosynthetic-reinforced stone column with vertical encasement length L exhibited a more uniform deformation rate along its length. For the vertical encasement length L/2, deformation was primarily localized in the unreinforced section.

3.3. Stress concentration ratio

The stress distribution between the stone column and the soil layer can be quantitatively described by the stress concentration ratio (SCR) (Li et al., 2023):

$$SCR = \frac{\sigma_c}{\sigma_s} \tag{3}$$

where σ_c represents the vertical stress borne by the stone column, and σ_s denotes the vertical stress borne by the surrounding soil. In this study, σ_c and σ_s are experimentally determined values, measured using earth pressure cells embedded at the top of the stone column and in the adjacent surrounding soil (Fig. 4). Fig. 11 illustrates the variation curve of the SCR with the settlement ratio (S/D) under different reinforcement conditions, in which the settlement (S) was recorded by pull wire displacement sensors (Fig. 4). The SCR exhibited fluctuations with increasing foundation settlement across all reinforcement scenarios. Specifically, the SCR values for vertical reinforcement and horizontal reinforcement ranged from 3.27 to 6.14 and 2.63 to 4.34, respectively. The maximum SCR for the combined reinforcement (L/2 + 2D/3) reached 5.84, all exceeding the SCR of the unreinforced stone column, indicating that reinforced columns can sustain greater stress.

Furthermore, the SCR value increased with decreasing reinforcement spacing and increasing reinforcement length, as these factors enhance the overall rigidity and integrity of the stone column. Notably, before the settlement reached 10 mm, the SCR showed significant increases across all columns. As settlement continued to increase, the SCR began to decline and gradually stabilized. This behaviour can be attributed to the initial downward movement of the stone column during loading, which caused rearrangement of the column filler, resulting in increased density and enhanced interlocking effects among the fillers, allowing the column to support greater stress. As the load and settlement further increased, the filler tended to move laterally toward the surrounding soil, leading to a gradual transfer of load to the surrounding soil. This resulted in interlocking effects not only among the fillers but also between the column and horizontal geosynthetics, enhancing friction and limiting lateral movement of the filler.

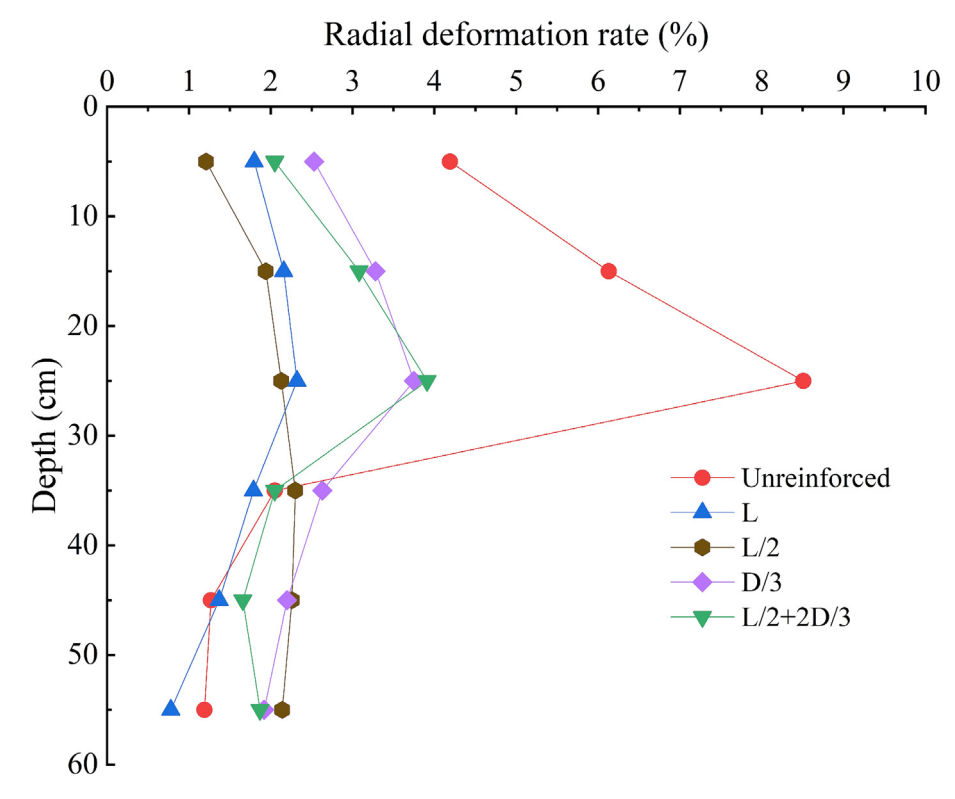


Fig. 10. Radial deformation rates of the column with different reinforcements.

Moreover, the SCR value was highest for the L-length encasement. This is due to the geotextile encasement limiting lateral stress transfer between the column and the soil, thereby reducing the column's dependence on the surrounding soil for bearing capacity. The vertical L-length reinforcement provided optimal integrity and additional lateral constraints among all reinforcement methods, which explains its superior peak and residual SCR value.

4. Conclusions

This study examined the performance of stone column foundations under various conditions using physical model tests. The bearing capacity and deformation characteristics of stone columns were examined under different vertical encasement lengths, horizontal reinforcement spacings, and combined reinforcement methods. The key findings are as follows:

(1) Compared to unreinforced stone columns, the bearing capacity of stone column foundations significantly improves with reinforcement. For horizontal reinforced stone column, the bearing capacity increases as the reinforcement spacing decreases. For vertical reinforced stone column, the bearing capacity increases with longer encasement lengths. The optimal combined reinforcement case is L/2 + 2D/3. Among the various methods, vertical reinforcement with full-length encasement exhibits the most substantial enhancement in bearing capacity.

- (2) Deformations primarily occur within the upper 3.5D depth of the column, with a concentration within 2.5D. Geosynthetics significantly limit the radial deformation of columns, allowing deformation to expand downward, resulting in increased deformation in the lower part of the column. Vertical reinforcement with full-length encasement demonstrates the best deformation uniformity, with a maximum radial deformation rate of only 2.1 % due to its superior rigidity and integrity.
- (3) Reinforcements that enhance foundation bearing capacity also improve the stress concentration ratio. As the encasement length increases and the reinforcement spacing decreases, the stress within the reinforced column rises, resulting in a more uniform stress concentration ratio along the depth during loading. The vertical reinforcement with full-length encasement exhibits the highest stress concentration ratio.
- (4) As the vertical load increases, the lateral stress on the column sides rises continuously at various depths. The lateral stress initially increases and then decreases from the top to the bottom of the column, peaking at a depth of 2.5D. This suggests that greater column deformation results in higher horizontal pressure on the surrounding soil.
- (5) Different reinforcement methods exhibit distinct effects on the stone column foundations, with full-length encased vertical reinforcement demonstrating the most significant enhancement in both bearing capacity and column deformation.

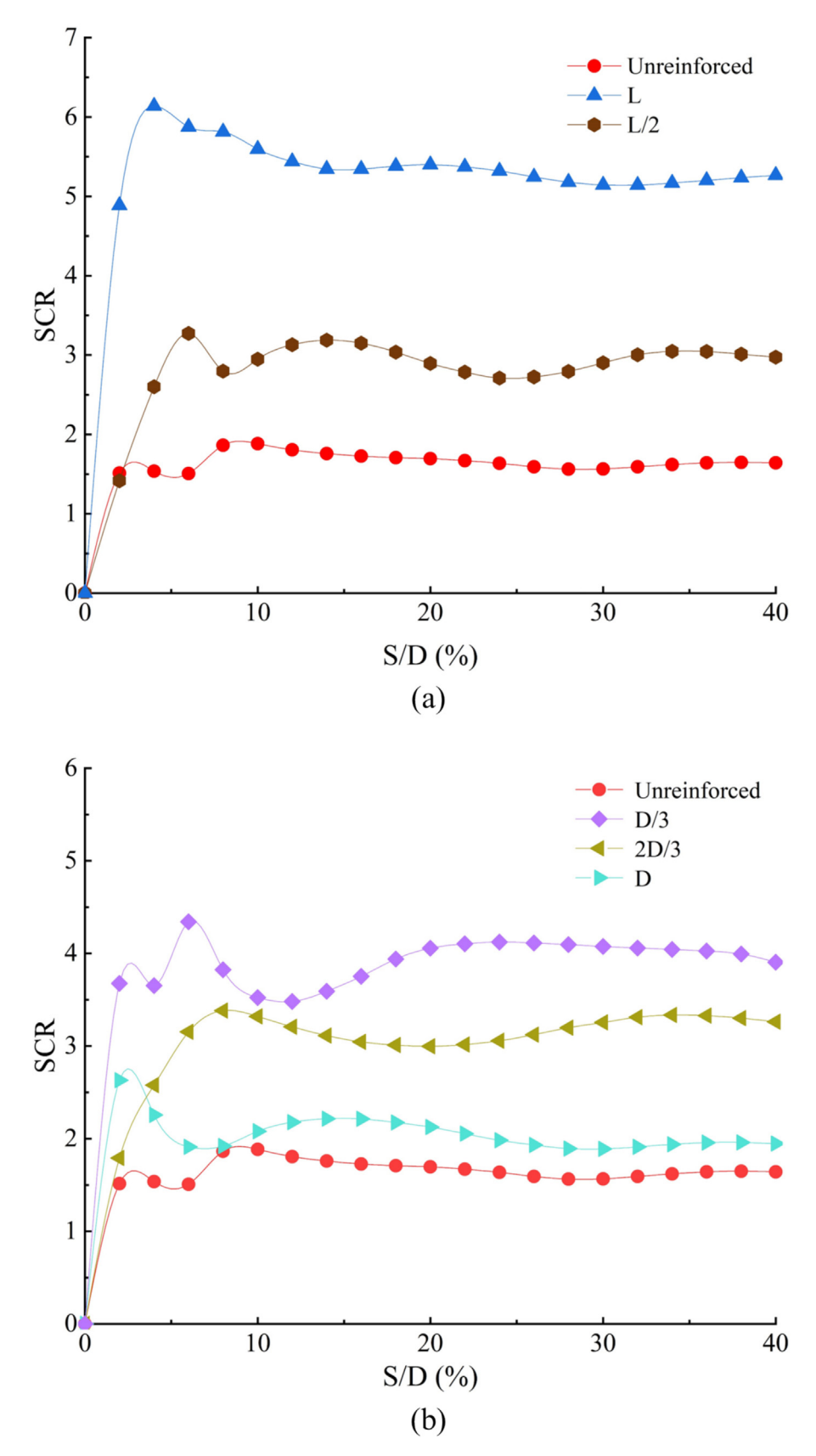


Fig. 11. SCR variation under (a) vertical reinforcements; (b) horizontal reinforcements; and (c) the optimal reinforcement methods.

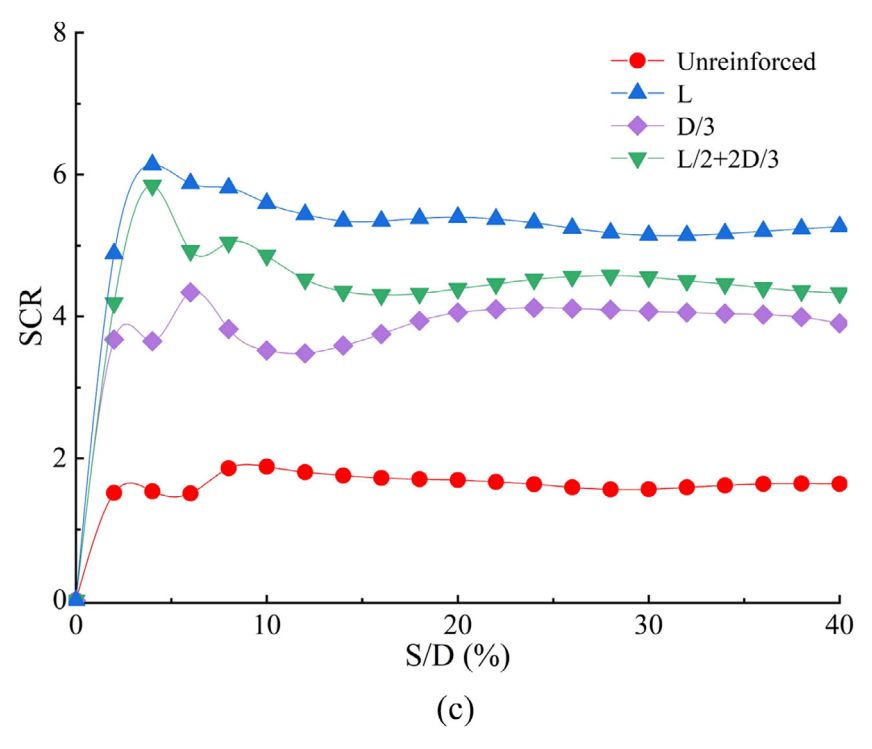


Fig 11. (continued)

CRediT authorship contribution statement

Lihua Li: Writing – review & editing, Validation, Supervision, Funding acquisition. Jinlin Li: Writing – review & editing, Methodology, Investigation, Data curation. Zhiqi Zhan: Writing – review & editing, Validation, Supervision, Investigation, Formal analysis, Data curation. Yilin Gui: Writing – review & editing, Validation. Juqiang Liu: Writing – original draft, Methodology.

Acknowledgments

The authors gratefully acknowledge the financial support from the Outstanding Young and Middle-aged Scientific and Technological Innovation Team Project of Higher Education Institutions in Hubei Province (T2023006), the Natural Science Fund for Creative Groups of Hubei Province (Grant No. 2024AFA009), and the National Natural Science Foundation of China (Grant No. 52278347).

References

Ali, K., Shahu, J., Sharma, K., 2012. Model tests on geosynthetic-reinforced stone columns: a comparative study. Geosynth. Int. 19 (4), 292–305.

Bazzazian Bonab, S., Lajevardi, S.H., Saba, H.R., Ghalandarzadeh, A., Mirhosseini, S.M., 2020. Experimental studies on single reinforced stone columns with various positions of geotextile. Innovative Inf. Solut. 5, 1–12. Benmebarek, S., Remadna, A., Benmebarek, N., 2018. Numerical modelling of stone column installation effects on performance of circular footing. Int. J. Geosynth. Ground Eng. 4, 1–15.

Cai, Z., Wang, F., Gao, C., He, N., Liu, X., Gong, B., Wu, Q., Li, P., Hu, Z., Ling, H., 2019. Standard for geotechnical testing method. General Institute of Water Conservancy and Hydropower Planning and Design, Ministry of Water Resources, Beijing, China.

Castro, J., 2014. Numerical modelling of stone columns beneath a rigid footing. Comput. Geotech. 60, 77–87.

Choo, J., 2018. Mohr–Coulomb plasticity for sands incorporating density effects without parameter calibration. Int. J. Numer. Anal. Meth. Geomech. 42 (18), 2193–2206.

Chummar, A.V., 1975. Closure to "bearing capacity theory from experimental results". J. Geotech. Eng. Div. 101 (1), 69.

Dash, S.K., Bora, M.C., 2013. Improved performance of soft clay foundations using stone columns and geocell-sand mattress. Geotext. Geomembr. 41, 26–35.

Deb, K., Samadhiya, N.K., Namdeo, J.B., 2011. Laboratory model studies on unreinforced and geogrid-reinforced sand bed over stone column-improved soft clay. Geotext. Geomembr. 29 (2), 190–196.

Debnath, P., Dey, A.K., 2017. Bearing capacity of reinforced and unreinforced sand beds over stone columns in soft clay. Geosynth. Int. 24 (6), 575–589.

Deshpande, T.D., Kumar, S., Begum, G., Basha, S., Rao, B.H., 2021. Analysis of railway embankment supported with geosynthetic-encased stone columns in soft clays: a case study. Int. J. Geosynth. Ground Eng. 7 (2), 43.

Dinarvand, R., Ardakani, A., 2018. Behavior of geosynthetic-encased granular column in silty sand soil by direct shear test. Amirkabir J. Civil Eng. 50 (5), 961–972.

Elsawy, M., 2013. Behaviour of soft ground improved by conventional and geogrid-encased stone columns, based on FEM study. Geosynth. Int. 20 (4), 276–285.

Ghazavi, M., Afshar, J.N., 2013. Bearing capacity of geosynthetic encased stone columns. Geotext. Geomembr. 38, 26–36.

- Ghazavi, M., Yamchi, A.E., Afshar, J.N., 2018. Bearing capacity of horizontally layered geosynthetic reinforced stone columns. Geotext. Geomembr. 46 (3), 312–318.
- Gniel, J., Bouazza, A., 2010. Construction of geogrid encased stone columns: a new proposal based on laboratory testing. Geotext. Geomembr. 28 (1), 108–118.
- Hasan, M., Samadhiya, N.K., 2017. Performance of geosynthetic-reinforced granular piles in soft clays: model tests and numerical analysis. Comput. Geotech. 87, 178–187.
- Hasan, M., Samadhiya, N.K., 2018. Soft soils improvement by granular piles reinforced with horizontal geogrid strips. Int. J. Geotech. Eng. 12 (1), 101–108.
- Hataf, N., Nabipour, N., Sadr, A., 2020. Experimental and numerical study on the bearing capacity of encased stone columns. Int. J. Geo-Eng. 11, 1–19.
- Indraratna, B., Ngo, N.T., Rujikiatkamjorn, C., Sloan, S.W., 2015. Coupled discrete element–finite difference method for analysing the load-deformation behaviour of a single stone column in soft soil. Comput. Geotech. 63, 267–278.
- Kulhawy, F.H. Mayne, P.W. 1990. Manual on estimating soil properties for foundation design.
- Lade, P.V., Duncan, J.M., 1975. Elastoplastic stress-strain theory for cohesionless soil. J. Geotech. Eng. Div. 101 (10), 1037–1053.
- Lajevardi, S., Shamsi, H., Hamidi, M., Enami, S., 2018. Numerical and experimental studies on single stone columns. Soil Mech. Found. Eng. 55, 340–345.
- Lees, A., Matthias, P., 2019. Bearing capacity of a geogrid-stabilised granular layer on clay. Ground Eng. 10.
- Li, L.-H., Cao, Y., Liu, J.-Q., Xiao, H.-L., Zhang, D.-F., Liu, Y.-M., 2023. Experimental study on load bearing performance of stone columns under different reinforcement methods. Chin. J. Rock Mech. Eng. 42.
- Malarvizhi, S., 2007. Comparative study on the behavior of encased stone column and conventional stone column. Soils Found. 47 (5), 873–885.
- Murugesan, S., Rajagopal, K., 2006. Geosynthetic-encased stone columns: numerical evaluation. Geotext. Geomembr. 24 (6), 349–358.
- Murugesan, S., Rajagopal, K., 2010. Studies on the behavior of single and group of geosynthetic encased stone columns. J. Geotech. Geoenviron. Eng. 136 (1), 129–139.
- Naeini, S.A., Gholampoor, N., 2019. Effect of geotextile encasement on the shear strength behavior of stone column-treated wet clays. Indian Geotechnical Journal 49, 292–303.
- Nazari Afshar, J., Ghazavi, M., 2014. Experimental studies on bearing capacity of geosynthetic reinforced stone columns. Arab. J. Sci. Eng. 39, 1559–1571.

- Orekanti, E.R., Dommaraju, G.V., 2019. Load-settlement response of geotextile encased laterally reinforced granular piles in expansive soil under compression. Int. J. Geosynth. Ground Eng. 5 (3), 17.
- Pereiro-Barceló, J., Bonet, J.L., Rueda-García, L., Ciurana-Tatay, Á., 2022. Behaviour of retrofited precast UHPC and Ni-Ti SMA columnto-foundation connection with CFRP wrapping layers. Constr. Build. Mater. 323 126536.
- Rathod, D., Abid, M.S., Vanapalli, S.K., 2021. Performance of polypropylene textile encased stone columns. Geotext. Geomembr. 49 (1), 222–242.
- Schweiger, H., Pande, G., 1986. Numerical analysis of stone column supported foundations. Comput. Geotech. 2 (6), 347–372.
- Shahu, J., Reddy, Y., 2011. Clayey soil reinforced with stone column group: model tests and analyses. J. Geotech. Geoenviron. Eng. 137 (12), 1265–1274.
- Sharma, R.S., Kumar, B.P., Nagendra, G., 2004. Compressive load response of granular piles reinforced with geogrids. Can. Geotech. J. 41 (1), 187–192.
- Tandel, Y.K., Solanki, C.H., Desai, A.K., 2014. Field behaviour geotextile reinforced sand column. Geomech. Eng 6 (2), 195–211.
- Thakur, A., Rawat, S., Gupta, A.K., 2021. Experimental and numerical investigation of load carrying capacity of vertically and horizontally reinforced floating stone column group. Geotech. Geol. Eng. 39, 3003– 3018.
- Van Impe, W.F. 1989. Soil improvement techniques and their evolution.
- Verma, S., Kumar, V., Priyadarshee, A., 2018. An experimental test study on ring footing resting on clay bed reinforced by stone column. Innovative Inf. Solut. 3, 1–16.
- Wu, C.-S., Hong, Y.-S., 2008. The behavior of a laminated reinforced granular column. Geotext. Geomembr. 26 (4), 302–316.
- Wu, C.-S., Hong, Y.-S., 2014. A simplified approach for evaluating the bearing performance of encased granular columns. Geotext. Geomembr. 42 (4), 339–347.
- Yoo, C., Lee, D., 2012. Performance of geogrid-encased stone columns in soft ground: full-scale load tests. Geosynth. Int. 19 (6), 480–490.
- Zhan, Z.Q., Zhou, C., Cui, Y.F., Liu, C.Q., 2025. Initiation and motion of rainfall-induced loose fill slope failure: New insights from the MPM. Eng. Geol. 346, 107909.
- Zhang, L., Zhao, M., 2015. Deformation analysis of geotextile-encased stone columns. Int. J. Geomech. 15 (3) 04014053.